Journal of Solid State Chemistry 242 (2016) 186–192

Contents lists available at ScienceDirect

Journal of Solid State Chemistry

journal homepage: www.elsevier.com/locate/jssc

A new family of metal borohydride guanidinate complexes: Synthesis, structures and hydrogen-storage properties

Hui Wu [a,*], Xiuquan Zhou [b], Efrain E. Rodriguez [b], Wei Zhou [a], Terrence J. Udovic [a], Taner Yildirim [a], John J. Rush [a,c]

[a] NIST Center for Neutron Research, National Institute of Standards and Technology, Gaithersburg, MD 20899-6102, USA
[b] Department of Chemistry & Biochemistry, University of Maryland, College Park, MD 20742-4454, USA
[c] Department of Materials Science and Engineering, University of Maryland, College Park, MD 20742-2115, USA

ARTICLE INFO

Article history:
Received 2 June 2016
Received in revised form
6 July 2016
Accepted 12 July 2016
Available online 15 July 2016

Keywords:
Borohydrides
Guanidine
Crystal structure determination
Neutron vibrational spectroscopy
Dehydrogenation
Thermodynamics

ABSTRACT

We report on a new class of complex hydrides: borohydride guanidinate complexes ($MBH_4{\cdot}nCN_3H_5$, M=Li, Mg, and Ca). They can be prepared via facile solid-state synthesis routes. Their crystal structures were successfully determined using a combination of X-ray diffraction, first-principles calculations and neutron vibrational spectroscopy. Among these compounds, $Mg(BH_4)_2{\cdot}6CN_3H_5$ is composed of large complex $Mg[CN_3H_5]_6^{2+}$ cations and surrounding BH_4^- ions, while $Ca(BH_4)_2{\cdot}2CN_3H_5$ possesses layers of corner-sharing $Ca[BH_4]_4(CN_3H_5)_2$ octahedra. Our dehydrogenation results show that ≈ 10 wt% hydrogen can be released from $MBH_4{\cdot}nCN_3H_5$ (M=Li, Mg, and Ca) at moderate temperatures with minimal ammonia and diborane contamination thanks to the synergistic effect of C-N bonds from guanidine and hydridic H from borohydrides leading to a weakening of the N-H bonds, thus impeding ammonia gas liberation. Further tuning the dehydrogenation with different cation species indicates that Mg$(BH_4)_2{\cdot}nCN_3H_5$ can exhibit the optimum properties with nearly thermally neutral dehydrogenation and very high purity hydrogen release.

Published by Elsevier Inc.

1. Introduction

Complex hydrides such as alkali and alkaline-earth metal borohydrides (MBH_4) and amides (MNH_2) have attracted much attention for hydrogen-storage applications due to their intriguing hydrogen-storage capacity and cycling ability [1–9]. Several systems, such as $Mg(BH_4)_2$ [10–12], have achieved full reversibility, although the process conditions (pressure and temperature) for their dehydrogenation and hydrogenation are higher than the DOE requirements due to their thermal stability. For other systems, decomposition at high temperatures leads to side reactions with concomitant toxic gas by-products, such as diborane and ammonia, which further prevent complete rehydrogenation due to loss of the B or N components in the systems [5,6]. One effective way to weaken the chemical bonds (lower dehydrogenation temperature) and facilitate preferential H_2 release (suppress by-product gases) is to develop systems with coexisting $H^{\delta+}$ and $H^{\delta-}$ because of the thermodynamically favorable recombination reaction of H's with opposite charges ($H^- + H^+ \rightarrow H_2$ $\Delta H = -17.37$ eV). For example, the MNH_2+MH system [13–17] has demonstrated significant potential for a reversible on-board hydrogen-storage material, albeit with some release of ammonia—a common difficulty of the amide compounds. Borohydride derivatives with coexisting $H^{\delta+}$ and $H^{\delta-}$ such as $M_{m+n}(BH_4)_m(NH_2)_n$ and $MBH_4{\cdot}nNH_3$ have also been developed with intriguing diverse crystal structural arrangements [18–25]. The net effect of introducing protic hydrogen into a borohydride system is a combination of the strength and polarity of M-H bonds and the attractive interaction between H's. Hence, the thermal stability, decomposition temperatures and purity of the released gases for such complex systems vary largely, depending on the electronegativity and polarizing power of the associated metal species. Furthermore, the endothermic decomposition of borohydrides upon ammoniating is touted to be exothermic, albeit with a lowered decomposition temperature by the formation of a stable B-N decomposition product, preventing a direct re-hydrogenation. Although in some cases, NH_3, with a lone electron pair available for bonding, can help stabilize hydrides profitably e.g., $Al(BH_4)_3{\cdot}6NH_3$ [26], the enthalpy change as a result of stabilizing these compounds is not sufficient to be the game changer for an endothermic dehydrogenation.

As part of this endeavor in developing new $H^{\delta+}$ and $H^{\delta-}$ co-containing complex hydrides, herein, we report the syntheses and detailed structural and property characterization of a new family of borohydride guanidinates $MBH_4{\cdot}nCN_3H_5$ (M=Li, Mg, and Ca),

* Corresponding author.
E-mail address: huiwu@nist.gov (H. Wu).

http://dx.doi.org/10.1016/j.jssc.2016.07.013
0022-4596/Published by Elsevier Inc.

aiming to explore new high-hydrogen-content compounds with potential applications for hydrogen storage. Introducing borohydrides with various metal species is desirable to induce more reactive H^- to combine effectively with H^+ in guanidine molecules as well as to adjust the N-H bond strength by metals with different electronegativities. Compared to CN_3H_5/MH or MCN_3H_4/MH composites in our previous study, these new borohydride guanidinate complexes with attractive hydrogen contents (> 10 wt%) exhibit high-purity hydrogen release at moderate temperatures. Particularly, compared to the previously reported borohydride ammoniates with exothermic dehydrogenation, $Mg(BH_4)_2{\cdot}2CN_3H_5$ and $Ca(BH_4)_2{\cdot}2CN_3H_5$ exhibit a nearly thermally neutral dehydrogenation, indicating that a full rehydrogenation is potentially promising.

2. Materials and methods

High-purity guanidine (CN_3H_5) and guanidinium borohydride ($[CN_3H_6][BH_4]$) were prepared using a modified method reported in the literature [27,28]. For synthesis of high-purity guanidine, stoichiometric amounts of Na metal and guanidinium carbonate (2:1 molar ratio) were separately dissolved in anhydrous ethanol in a nitrogen-filled glove box. The two solutions were mixed and filtered to yield a colorless ethanol solution of guanidine. Solid guanidine was obtained by evaporating ethanol under vacuum, and the product was further purified by sublimation on a Schlenk line. The yield for the final purified product was about 60%. For synthesis of high-purity guanidinium borohydride, in a typical reaction, 30 mmol of sodium borohydride and 30 mmol guanidine hydrochloride were mixed with 20 mL of anhydrous Tetrahydrofuran (THF) in a flask under Ar flow on a Schlenk line. The mixture was stirred for 18 h at room temperature and subsequently filtered using a Buchner funnel under vacuum. Pure guanidinium borohydride was recovered by evaporating the collected filtrate under vacuum on a Schlenk line. The yield for the product was about 80%. Borohydride ($LiBH_4$, $Mg(BH_4)_2$ and $Ca(BH_4)_2$, > 95% purity) and metal hydride (LiH, MgH_2 and CaH_2, > 99% purity) precursors were purchased from Sigma-Aldrich. The $MBH_4{\cdot}nCN_3H_5$ compounds were then synthesized by grinding corresponding molar ratios of borohydride and guanidine in an agate mortar with a pestle or by ball milling the MH-$CN_3H_6BH_4$ powder mixtures using a Fritsch Pulverisette 7 planetary mill at 200 rpm for 3 h. All sample handling was performed in a He-filled glovebox due to the air-sensitivity of these complex hydrides.

Phase identification and equilibrium were monitored on samples sealed in glass capillaries using a Rigaku X-ray diffractometer with a Cu K_α source. Data for structural studies were collected over 24 h at room temperature in the 2θ range of 5–70° with a step size of 0.02°. Rietveld structural refinements were done using the GSAS package [29]. Neutron vibrational spectra (NVS) were measured at 5 K using the BT-4 Filter-Analyzer Neutron Spectrometer (FANS) at the NIST Center for Neutron Research, with the Cu(220) monochromator under conditions that provided energy resolutions of 2–4.5% over the vibrational energy range probed.

Thermogravimetric analysis (TGA) measurements with simultaneous differential scanning calorimetry (DSC) were made using a Netzsch (STA 449 *F1 Jupiter*) TGA-DSC instrument under He flow with Al sample pans and temperature ramp rates of 2 °C/min. Temperature readings were estimated to be accurate to within ± 1 °C. Temperature-programmed-desorption (TPD) measurements were performed on a Sieverts-type apparatus described previously [30]. Mass spectrometry (MS) measurements were conducted using a Hiden RGA mass spectrometer. TPD and MS measurements were performed from room temperature to 400 °C at a ramping rate of 2 °C/min.

First-principles calculations based on density-functional theory (DFT) were performed with the PWSCF package [31]. We used a Vanderbilt-type ultrasoft potential with Perdew-Burke-Ernzerhof exchange correlation. A cutoff energy of 544 eV was found to be enough for the total energy to converge within 0.5 meV/atom. Car-Parrinello molecular dynamics simulations [32] were used to help in searching for the most likely crystal structures. Structure optimizations on the candidate structures were further performed with respect to atomic positions, with the lattice parameters fixed at the experimental values. Lattice dynamics calculations were then performed on the relaxed structures using the supercell method with finite displacements [33].

3. Results and discussion

3.1. Syntheses and crystal structures of borohydride guanidinates

Borohydride guanidinates were first prepared by mixing $LiBH_4$, $Mg(BH_4)_2$ and $Ca(BH_4)_2$ with guanidine (CN_3H_5) powder in 1:1, 1:2 and 1:2 molar ratios, respectively. Combination of CN_3H_5 and $LiBH_4$ generates a translucent slurry with a featureless X-ray diffraction (XRD) pattern, indicating the formation of an amorphous phase, while mixing guanidine with $Mg(BH_4)_2$ and $Ca(BH_4)_2$ produces crystalline compounds. An alternative synthesis route was also conducted by mixing LiH, MgH_2 and CaH_2 with guanidinium borohydride ($[CN_3H_6][BH_4]$) powders in 1:1, 1:2, and 1:2 molar ratios respectively. The 1:1 ratio of the LiH/$[CN_3H_6][BH_4]$ mixture again led to the formation of an amorphous slurry. No reaction was found after ball milling the 1:2 ratio of MgH_2/$[CN_3H_6][BH_4]$ mixtures, whereas similar XRD patterns were observed for both the ball-milled product of CaH_2/2$[CN_3H_6][BH_4]$ mixtures and the ground $Ca(BH_4)_2$/2CN_3H_5. The XRD peaks could be indexed using an orthorhombic *Pna2₁* cell (No. 33) with lattice parameters of a=8.329 Å, b=8.413 Å, and c=14.201 Å. With the indexed lattice parameters, the crystal structure of calcium borohydride guanidinate with a stoichiometry of $Ca(CN_3H_5)_2(BH_4)_2$ was then solved using combined direct space methods and first-principles molecular dynamics simulated annealing. The determined composition indicates that by ball milling CaH_2 and $[CN_3H_6][BH_4]$, the hydridic H^- from CaH_2 could deprotonate the guanidinium cation $[CN_3H_6]^+$ to form the neutral guanidine molecule (CN_3H_5) with a release of H_2. The remaining BH_4^- anions and Ca^{2+} cations in the system then combine with the guanidine molecules formed in-situ and produce $Ca(CN_3H_5)_2(BH_4)_2$ (Eq. (1)), which is the same product as starting directly from borohydride and guanidine (Eq. (2)).

$$MH_n + n[CN_3H_6][BH_4] \rightarrow M(BH_4)_n{\cdot}nCN_3H_5 + nH_2 \quad (1)$$

$$M(BH_4)_n + nCN_3H_5 \rightarrow M(BH_4)_n{\cdot}nCN_3H_5 \quad (2)$$

Little reaction observed between MgH_2 and $[CN_3H_6][BH_4]$ is probably due to the less reactive MgH_2 precursor, while both synthetic routes from different precursors confirm the amorphous nature of $LiBH_4{\cdot}CN_3H_5$.

The major peaks of the XRD pattern (Fig. S1 in the appendix) for the crystalline product of $Mg(BH_4)_2$/2CN_3H_5 (with a small amount of extra $Mg(BH_4)_2$) can be indexed into a hexagonal *R-3* cell with a=11.819 Å and c=14.101 Å. By comparing to the lattice volumes of the precursors $Mg(BH_4)_2$ and CN_3H_5, the stoichiometry of the new phase is evaluated to be $Mg(CN_3H_5)_6(BH_4)_2$, assuming three formula units per unit cell, which is consistent with *R-3* extinction. A further test on mixing a 1:6 molar ratio of $Mg(BH_4)_2$ and CN_3H_5 generates a pure $Mg(CN_3H_5)_6(BH_4)_2$ phase. While the quality and insensitivity of XRD do not allow accurate determination of atomic positions for lightweight H, the crystal structure

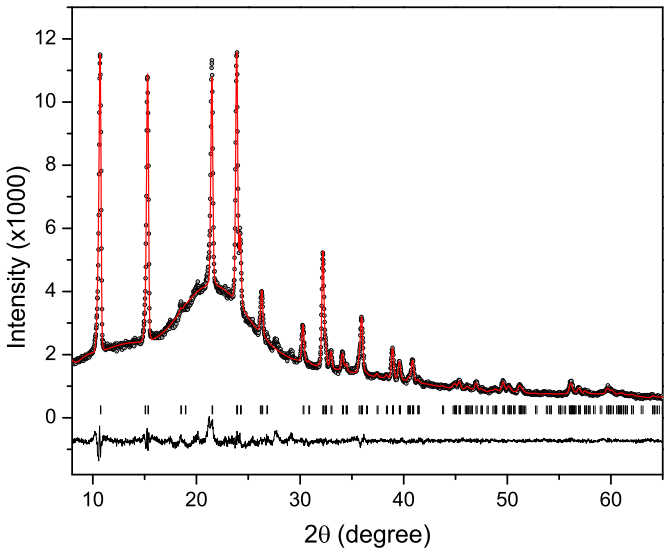

Fig. 1. Experimental (circles), calculated (line), and difference (line below observed and calculated patterns) XRD profiles for $Mg(CN_3H_5)_6(BH_4)_2$ at room temperature (CuKa radiation). Vertical bars indicate the calculated positions of Bragg peaks.

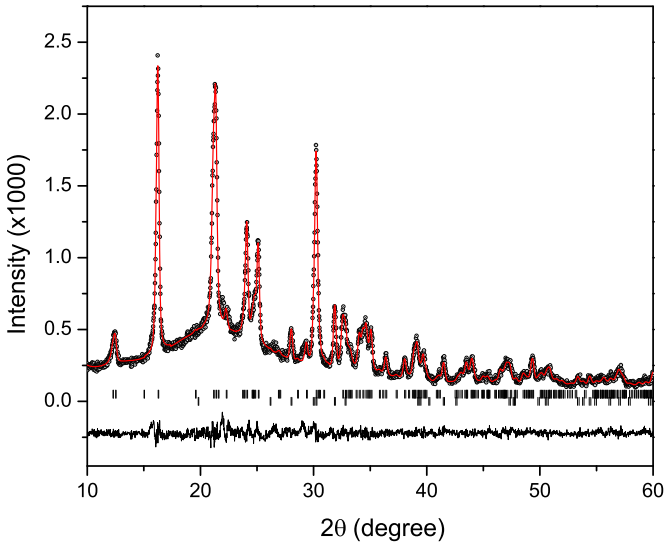

Fig. 2. Experimental (circles), calculated (line), and difference (line below observed and calculated patterns) XRD profiles for $Ca(CN_3H_5)_2(BH_4)_2$ at room temperature (CuKa radiation). Vertical bars indicate the calculated positions of Bragg peaks from $Ca(CN_3H_5)_2(BH_4)_2$ (94.92(4) wt%) and unreacted precursor CaH_2 (5.08(7) wt%).

of $Mg(CN_3H_5)_6(BH_4)_2$ was then solved similarly by the direct space method with the help of molecular dynamics simulations to derive the structure models with favorable BH_4^- and CN_3H_5 orientations. Rietveld structural refinements for both $Mg[CN_3H_5]_6(BH_4)_2$ and $Ca(CN_3H_5)_2(BH_4)_2$ were then performed using these structure models. It can be seen that all the XRD peaks of $Mg[CN_3H_5]_6(BH_4)_2$ and $Ca(CN_3H_5)_2(BH_4)_2$ phases can be well fitted using the determined structure models (Figs. 1 and 2) with agreement factors of $R_{wp}=0.0360$ and $R_p=0.0273$ for $Mg[CN_3H_5]_6(BH_4)_2$ and $R_{wp}=0.0511$ and $R_p=0.0430$ for $Ca(CN_3H_5)_2(BH_4)_2$, which strongly supports the validity of our structure solutions. The detailed structural information is given in the crystallographic information files (CIFs) (CSD-430849 and CSD-430850) in the ICSD database.

The fully relaxed crystal structures for $Mg(CN_3H_5)_6(BH_4)_2$ and $Ca(CN_3H_5)_2(BH_4)_2$ are shown in Fig. 3. Note that the refinement based on laboratory X-ray data cannot provide highly accurate atomic coordinates especially for H, thus fully relaxed structure from the First-principles calculations is used in the bond length discussion below. In the structure of $Mg(CN_3H_5)_6(BH_4)_2$, each Mg^{2+} cation is coordinated by six CN_3H_5 molecules via the N atoms of the –NH imino groups, forming a large hexaguanidinemagnesium(II) complex cation, $Mg[CN_3H_5]_6^{2+}$. For each CN_3H_5 molecule ligand, upon bonding with Mg^{2+}, both the C-N_{imino} (1.316 Å) and C-N_{amino} (1.376 Å) bond lengths are slightly shorter than those in $LiCN_3H_4$ (1.33 Å and 1.41 Å) and $NaCN_3H_4$ (1.34 Å and 1.41 Å). The Mg-N bond length is 2.238 Å, which is practically the same as those in ionic hexacoordinated ammine magnesium complexes $Mg(NH_3)_6Cl_2$ (2.197 Å), [34] $Li_2Mg(NH_3)_6(BH_4)_4$ (2.239 Å) [35] and $Mg_2(NH_3)_6(NH_2BH_3)_4$ (2.217 Å) [36]. This giant complex cation $Mg[CN_3H_5]_6^{2+}$ is then surrounded by fourteen BH_4^- ions (Fig. 3). The $NH^{\delta+\cdots\delta-}HB$ distances range from 1.94 Å to 2.40 Å, which are sufficiently short to build dihydrogen bonds.

In contrast to the ionic $Mg[CN_3H_5]_6(BH_4)_2$ structure, in $Ca(CN_3H_5)_2(BH_4)_2$, each Ca^{2+} is octahedrally coordinated with four BH_4^- ions and two CN_3H_5 molecules, forming a polymeric structure, which has layers of corner-sharing $Ca[BH_4]_4(CN_3H_5)_2$ octahedra with bridged BH_4^- ions and CN_3H_5 ligands in the *trans* position. These layers are then interlocked by dihydrogen bonding between the CN_3H_5 vertices in one layer and bridging BH_4^- ions in the adjacent layers with $NH^{\delta+\cdots\delta-}HB$ distances in the range of 1.96 Å to 2.41 Å. The average C-N_{imino} (1.323 Å) and C-N_{amino} (1.362 Å) bond lengths are similar to those in $Mg[CN_3H_5]_6(BH_4)_2$. The average Ca-N bond distance is 2.424 Å, compatible with those in $Ca(NH_3)_2(BH_4)_2$ (2.49 Å) [37] and $Ca(NH_3)(NH_2BH_3)_2$ (2.42 Å) [38]. Different from the complex $Mg[CN_3H_5]_6^{2+}$ cation in $Mg[CN_3H_5]_6(BH_4)_2$, the Ca^{2+} cations in $Ca(CN_3H_5)_2(BH_4)_2$ exist in the simple cation form and directly contact with the hydridic H's from the surrounding BH_4^- ions. The distances between Ca and the nearby H's of BH_4^- are 2.386–2.658 Å, slightly shorter than those in $Ca(NH_3)_2(BH_4)_2$ (2.41–2.75 Å).

Neutron vibrational spectra were measured for $Ca(CN_3H_5)_2(BH_4)_2$ (Fig. 4), which directly reflect the vibrational density of states and are particularly sensitive to the vibrational modes related to hydrogen, whose positions cannot be determined from X-ray diffraction. The first-principles calculated NVS based on the relaxed structural model with the optimum CN_3H_5 and BH_4^- orientations are also shown in Fig. 4. Note it is typical for the DFT-derived phonon energies to deviate by around $\pm 5\%$ with respect to the experimentally observed energies, depending on the functional used. Compared to the calculated NVS, the observed neutron vibrational modes significantly smear out, especially for the modes round 100 meV. From the calculations, these are corresponding to the –NH imino-group related vibrational modes. Moreover, the –NH group-related modes are not present in the NVS collected on the $[CN_3H_6][BH_4]$ precursor (Fig. S2), which does not possess an imino group. Therefore, the smearing out of these –NH related modes in $Ca(CN_3H_5)_2(BH_4)_2$ may indicate a certain degree of disorder of the CN_3H_5 molecules in the actual crystal structure, i.e., the H's very likely distribute randomly with a 5/6 occupancy at each hydrogen position (meaning that the –NH imino group can be along either of the three C-N directions in the CN_3H_5 groups). From the calculations, the phonon modes in the range of 5–25 meV (1 meV $\approx 8.066\ cm^{-1}$) are from the lattice collective modes. Phone modes in the range of 25–40 meV are librations of CN_3H_5 and BH_4. Strong modes at 46–58 meV and 97–103 meV are the wagging modes of the N-H bond in $–NH_2$ groups and N-H groups, respectively, which are diffusive in the experimental NVS. Phonon modes at 64–72 meV and 89–92 meV are the oscillation and wagging modes from C-N bonds. Modes at 74–81 meV are from N-H rotations. C-N stretching modes are at 121 meV. Phonon modes in the range of 129–162 meV are the bending and deformation of BH_4 and CN_3H_5. Besides the disorder-induced smearing of the –NH/$–NH_2$ related phonon modes, the remaining

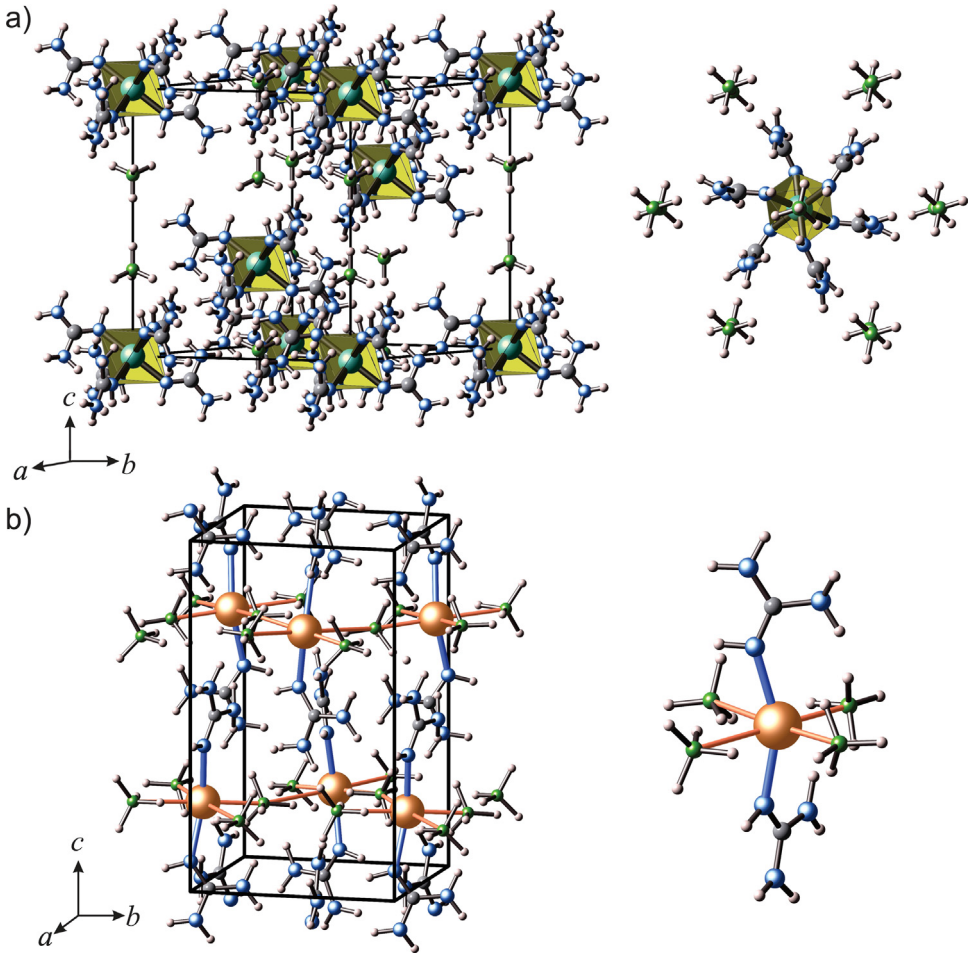

Fig. 3. Crystal structures of $Mg(CN_3H_5)_6(BH_4)_2$ and $Ca(CN_3H_5)_2(BH_4)_2$ (left column) and (right column) different local cation coordination environments. Mg, Ca, C, N, B and H are represented by light green, orange, grey, blue, green and white spheres, respectively. (For interpretation of the references to color in this figure legend, the reader is referred to the web version of this article.)

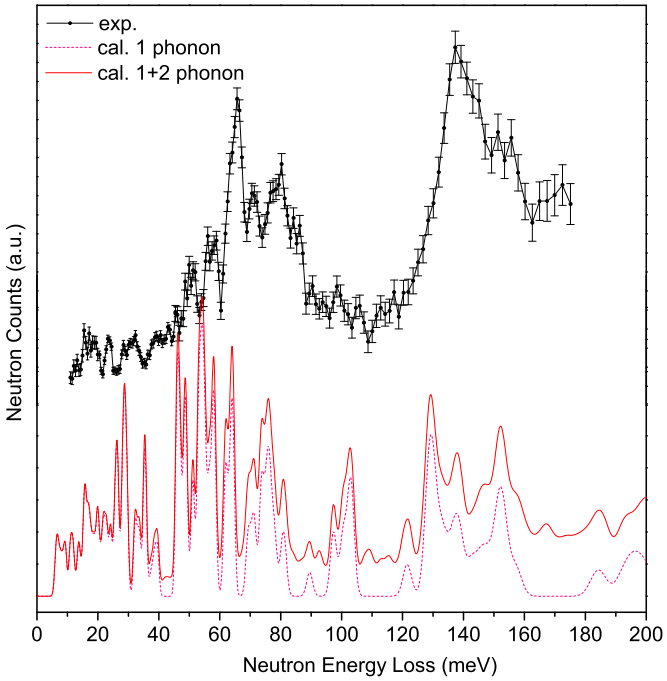

Fig. 4. Neutron vibrational Spectra and the calculated phonon modes of Ca $(CN_3H_5)_2(BH_4)_2$.

modes in the NVS spectra are in reasonable agreement with the calculated spectra, indicating the validity of the overall determined crystal structure framework and the atomic positions of the heavier elements other than H.

3.2. *Hydrogen-storage properties of $MBH_4{\cdot}nCN_3H_5$*

In order to investigate the effect of cation species on hydrogen-storage properties, all three borohydride guanidinates ($M(BH_4)_n{\cdot}nCN_3H_5$) were measured, although $LiBH_4{\cdot}CN_3H_5$ cannot form a crystalline phase. In addition, for magnesium borohydride guanidinate, dehydrogenation behavior was measured on the samples with a $Mg(BH_4)_2{\cdot}2CN_3H_5$ composition in addition to $Mg[CN_3H_5]_6(BH_4)_2$ in order to pair the hydridic and protic H's and minimize the by-product gases. The volumetric TPD measurements up to 400 °C were first performed (Fig. 5 and Fig. S3). $LiBH_4{\cdot}CN_3H_5$ releases ~4 equiv. of H_2 per mole hydride, while $Mg(BH_4)_2{\cdot}2CN_3H_5$ and $Ca(BH_4)_2{\cdot}2CN_3H_5$ liberate ~8 equiv. of H_2 per mole hydride, consistent with the available amount of hydridic H from each borohydride. The initial hydrogen-release temperature for these three borohydride guanidinates is as low as ~85 °C for $Mg(BH_4)_2{\cdot}2CN_3H_5$ and increases with cation species in a sequence of Mg < Ca < Li. Both $Mg(BH_4)_2{\cdot}2CN_3H_5$ and $Ca(BH_4)_2{\cdot}2CN_3H_5$ dehydrogenate in a two-step profile and release all H's below 300 °C, while $LiBH_4{\cdot}CN_3H_5$ exhibits a complicated dehydrogenation profile and gives off all H's below 250 °C. Decomposition of these borohydride guanidinates were also measured on a gravimetric scale.

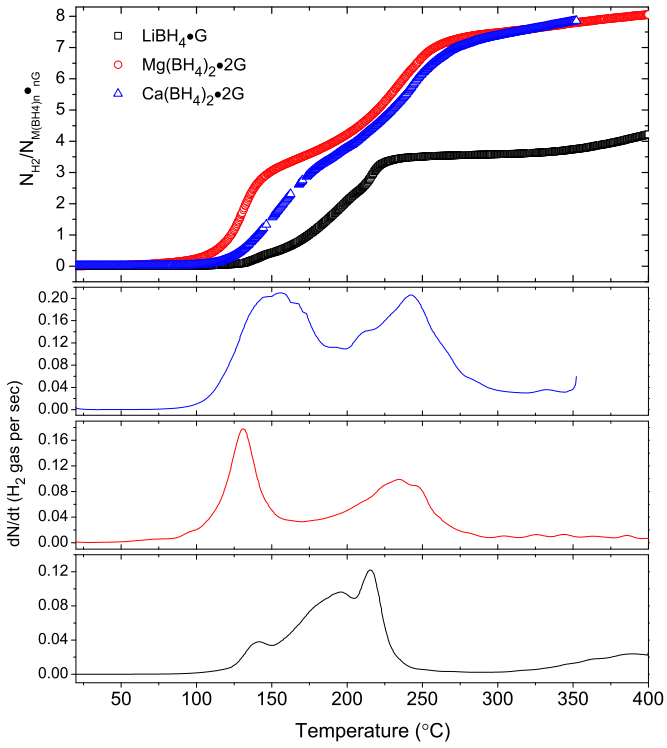

Fig. 5. TPD results of $M(BH_4)_n{\cdot}nCN_3H_5$ (M=Li, Mg, and Ca) with 2 °C/min heating rate to 400 °C. The amount of H_2 gas released (top panel) has been normalized as n (mol H_2 gas)/mol $M(BH_4)_n{\cdot}nCN_3H_5$.

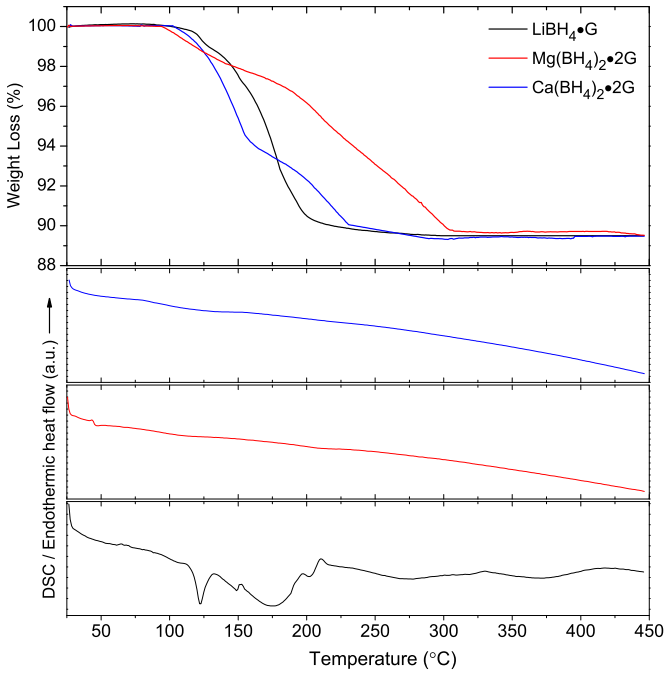

Fig. 6. TGA weight loss and the simultaneous DSC results for $M(BH_4)_n{\cdot}nCN_3H_5$ (M=Li, Mg, and Ca) with 2 °C/min heating rate to 450 °C.

From TGA results (Fig. 6) in the same temperature ranges, about 10.5, 10.3, and 10.6% of weight losses were observed for $LiBH_4{\cdot}CN_3H_5$, $Mg(BH_4)_2{\cdot}2CN_3H_5$ and $Ca(BH_4)_2{\cdot}2CN_3H_5$, respectively, which are compatible to the H contents of these hydrides. The simultaneous differential scanning calorimetry (DSC) measurements (Fig. 6) indicate that the decomposition of $LiBH_4{\cdot}CN_3H_5$ is exothermic, which is the same as other lithium borohydride ammoniates [39,40] or amide complexes, [18] while in contrast,

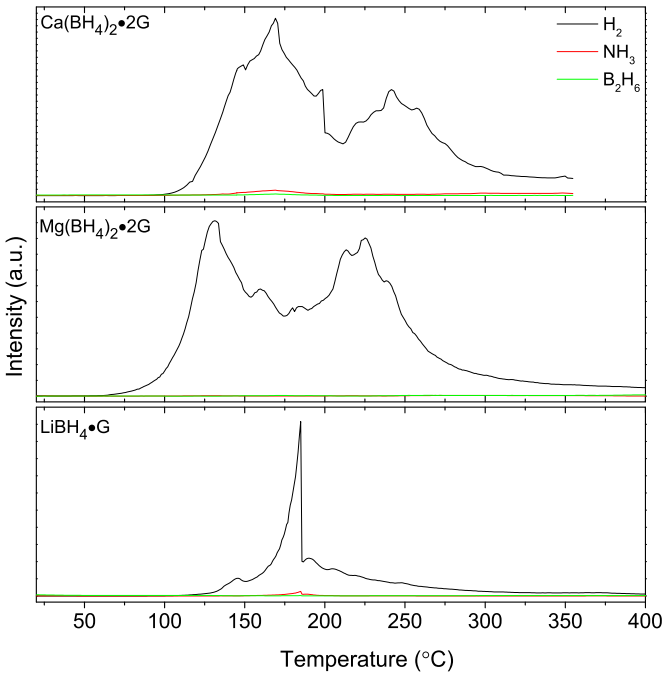

Fig. 7. MS from decomposition of $M(BH_4)_n{\cdot}nCN_3H_5$ (M=Li, Mg, and Ca) with 2 °C/min heating rate to 400 °C.

$Mg(BH_4)_2{\cdot}2CN_3H_5$ and $Ca(BH_4)_2{\cdot}2CN_3H_5$ decompose almost thermally neutral. This indicates that an even lower-temperature hydrogen release for these two compounds may be viable if the kinetic barriers can be overcome by catalytic modification.

The purity of gases released from the borohydride guanidinates was further inspected by a mass spectrometer (Fig. 7 and Fig. S4). It can be seen from Fig. 7 that $LiBH_4{\cdot}CN_3H_5$, $Mg(BH_4)_2{\cdot}2CN_3H_5$ and $Ca(BH_4)_2{\cdot}2CN_3H_5$ are able to release H_2 with minimized by-product gases such as ammonia (NH_3) and diborane (B_2H_6). In particular, $Mg(BH_4)_2{\cdot}2CN_3H_5$ releases very high purity H_2 with nearly no observable NH_3 and B_2H_6. XRD patterns collected after decomposition of $Mg(BH_4)_2{\cdot}2CN_3H_5$ and $Ca(BH_4)_2{\cdot}2CN_3H_5$ show broad lumps, indicating the formation of poorly crystalline products (Figs. S5 and S6). While for $LiBH_4{\cdot}CN_3H_5$, besides the amorphous lump, the XRD pattern (Fig. S7) of the post-desorption sample reveals the formation of a crystalline Li_2CN_2 phase. This suggests that with different cations these compounds may dehydrogenate via different reaction pathways. FTIR spectra (Fig. 8 and Fig. S8) collected on the dehydrogenation product of these compounds indicated the smearing of B-H and N-H bond vibrations after decomposition, confirming the dehydrogenation reactions between $H^{\delta-}$ from BH_4^- and $H^{\delta+}$ from CN_3H_5. For all three compounds after decomposition, there is a weak diffusive IR mode at 790–800 cm^{-1} (Fig. S8) whose position is in accordance with those attributed to the B-N stretching motion [41]. The attribution of this spectral line is also in the frequency range of the N-H wagging modes as shown in Fig. 8. Since CN_3H_5 has one more H compared to BH_4^-, there are still some –NH imino groups remaining in the decomposition products, as shown by the N-H stretching modes in the frequency range of 3100–3400 cm^{-1}. Therefore, the formation of B-N products during dehydrogenation is not very unambiguous. Attempts to rehydrogenate the decomposition products of $Mg(BH_4)_2{\cdot}2CN_3H_5$ and $Ca(BH_4)_2{\cdot}2CN_3H_5$ at 350 °C and 50 bar of H_2 were unsuccessful, probably due to the amorphous nature of the dehydrogenation residues. Amorphous boron and other B_xH_y polymers have been observed in the hydrogen sorption/desorption cycle of borohydrides and are proposed to act as boron sinks, further hindering their reversibility by

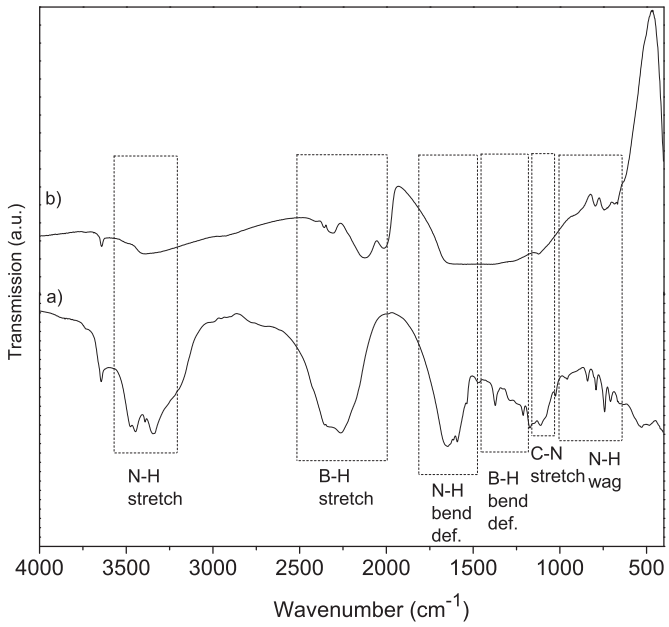

Fig. 8. FTIR results of $Ca(BH_4)_2{\cdot}2CN_3H_5$: (a) as-synthesized sample and (b) decomposition residue after TPD desorption measurement up to 400 °C.

direct pressurizing [42]. A chemical route for rehydrogenation for these compounds is still possible.

In the current study, the formation of Li_2CN_2 in the decomposition products of $LiBH_4{\cdot}CN_3H_5$ suggests that CN_3H_5 may partially dissociate from Li^+ first due to the weaker interaction between CN_3H_5 and Li^+ compared to Mg^{2+} or Ca^{2+}, and then decompose first via a direct H^-/H^+ recombination reaction at low temperature and then deammoniate and dehydrogenate via an ammonia-mediated mechanism at higher temperatures similar to the decomposition of $LiNH_2$ [43,44]. The deammoniation process produces Li_2CN_2 and ammonia. Such different capabilities on holding the coordinated ligands by cations with different electronegativities have also been observed in previous studies on numerous borohydride ammoniates and hydrazinates. For example, cations with higher electronegativity and/or high polarizing power are able to strongly bind to the coordinated ligands so that the protic H^+ of the ligands can directly react with the hydridic H^- of BH_4^- at high temperature, e.g. $Li_2Al(NH_3)_6(BH_4)_5$ [45] and $Mg(BH_4)_2{\cdot}2N_2H_4$, [46] whereas borohydrides with cations of lower electronegativity lose part or all of these volatile coordinated molecular ligands under the same condition, e.g. $LiBH_4{\cdot}NH_3$ [40] and $NaBH_4{\cdot}N_2H_4$ [47]. While it is worth noting that the appearance of Li_2CN_2 suggests some deammoniation in $LiBH_4{\cdot}CN_3H_5$, the amount of ammonia observed in the released gases is significantly less than those of $LiBH_4{\cdot}NH_3$, [40] $Li_{m+n}(BH_4)_m(NH_2)_n$ [18] and $LiBH_4{\cdot}nN_2H_4$ [47]. Evidently, in $LiBH_4{\cdot}CN_3H_5$, besides the common Li-ligand interactions as observed in other ligand-coordinated $LiBH_4$ complex compounds, the presence of the strong C-N bonds in CN_3H_5 play a marked role in impeding ammonia liberation from the system. In addition, although the C-N bond (305 kJ mol^{-1}) is weaker than the N-H bond (386 kJ mol^{-1}) in the CN_3H_5 molecule alone, in borohydride guanidinates, the N-H bonds are effectively weakened by the dihydrogen bonding with $^{\delta-}$H-B as evidenced by the reduced initial dehydrogenation temperatures and the minimized ammonia release in $LiBH_4{\cdot}CN_3H_5$ (~110 °C) compared to CN_3H_5 (~185 °C) or $LiCN_3H_4$ (~235 °C).

The more reactive hydridic H^- of borohydrides compared to those of metal hydrides can significantly boost the direct H^-/H^+ recombination reaction so as to lower the decomposition temperatures as well as suppress the ammonia gas release compared to the CN_3H_5/5LiH or $LiCN_3H_4$/4LiH composite. Furthermore, cations with higher electronegativity such as Mg^{2+} have also proven to proficiently reduce the N-H bond strength and thus decrease the dehydrogenation temperatures of amide compounds [48]. The observed lower dehydrogenation temperatures and higher H_2 purity of $Mg(BH_4)_2{\cdot}2CN_3H_5$ compared to $LiBH_4{\cdot}CN_3H_5$ in the current study are in line with the previous calculations [48] and experimental observations [14]. Finally, different from the endothermic decomposition of the CN_3H_5/5LiH composite, $LiBH_4{\cdot}CN_3H_5$ decomposes exothermically. This is likely due to the formation of stable B-N decomposition products similar to those of $LiBH_4{\cdot}NH_3$ [40], $Li_{m+n}(BH_4)_m(NH_2)_n$ [18] and $LiBH_4{\cdot}nN_2H_4$ [48]. The thermally neutral decomposition of $Mg(BH_4)_2{\cdot}2CN_3H_5$ and $Ca(BH_4)_2{\cdot}2CN_3H_5$ may be the collective effect the endothermic dehydrogenation and exothermic formation of possible B-N or amorphous B decomposition products.

Borohydride guanidinates ($MBH_4{\cdot}nCN_3H_5$) are a new family of high-H capacity complex hydrides containing non-volatile protic H components. Compared to $MBH_4{\cdot}nNH_3$, $MBH_4{\cdot}nN_2H_4$ and $M_{m+n}(BH_4)_m(NH_2)_n$, the strong C-N bonds in guanidine ligands can help hinder the liberation of the volatile ammonia or hydrazine gas, even for cations with lower electronegativity, e.g. Li^+, which usually cannot retain ligands strongly enough. On the other hand, the presence of reactive BH_4^- helps weaken N-H bonds in guanidine molecules and foster a direct H^+/H^- combination reaction with lower temperature and higher H_2 purity. Besides the collective benefit of the coexisting guanidine and BH_4^-, adjustment of cation species can further tune the hydrogen-storage properties of these compounds. As a result, $Mg(BH_4)_2{\cdot}2CN_3H_5$ with a more strongly electronegative cation, which can not only tighten up the ligands in the structure but also weaken the N-H bond strength, was found to exhibit the best hydrogen-storage properties among the three borohydride guanidinates studied here, with the lowest starting decomposition temperature, highest H_2 purity and nearly thermally neutral dehydrogenation.

4. Conclusions

A new family of high-H-content complex hydrides, borohydride guanidinates ($MBH_4{\cdot}nCN_3H_5$) were successfully developed by reacting guanidine (CN_3H_5) with borohydrides (MBH_4) or reacting guanidinium borohydride ($[CN_3H_6][BH_4]$) with metal hydrides (MH). The crystal structures of the two crystalline phases, formulated as $Mg[CN_3H_5]_6(BH_4)_2$ and $Ca(CN_3H_5)_2(BH_4)_2$, were determined using combined XRD and first-principles calculations. $LiBH_4{\cdot}CN_3H_5$, $Mg(BH_4)_2{\cdot}2CN_3H_5$ and $Ca(BH_4)_2{\cdot}2CN_3H_5$ release 4, 8 and 8 equiv. H_2 ($\approx$ 10 wt% H) with minimal ammonia and diborane contamination thanks to the synergistic effect of the C-N bond from guanidine and hydridic H from borohydrides. Dehydrogenation can be further tailored by varying the cation species. In particular, $Mg(BH_4)_2{\cdot}2CN_3H_5$ exhibits optimal hydrogen liberation with very high purity and a near neutral heat of dehydrogenation.

Appendix: Supplementary material

Supplementary data (extra structure and property characterizations associated with this article) can be found in the online version at http://dx.doi.org/10.1016/j.jssc.2016.xx.xxx. Crystallographic data (CIFs) of $Mg(CN_3H_5)_6(BH_4)_2$ and $Ca(CN_3H_5)_2(BH_4)_2$ can be found in ICSD database with number CSD-430849 and CSD-430850.

Funding sources

This work was partially supported by the DOE-EERE Grant no. DE-EE0002978 (T.J.U.).

Notes

Certain commercial suppliers are identified in this paper to foster understanding. Such identification does not imply recommendation or endorsement by the NIST.

Acknowledgments

We would like to thank Dr. Qiang Ye (NCNR, NIST) for his assistance with the mass spectrometer setup.

Appendix A. Supplementary material

Supplementary data associated with this article can be found in the online version at http://dx.doi.org/10.1016/j.jssc.2016.07.013.

References

[1] J. Vajo, S. Skeith, F. Mertens, Reversible storage of hydrogen in destabilized $LiBH_4$, J. Phys. Chem. B 109 (2005) 3719–3722.
[2] F. Pinkerton, M. Meyer, G. Meisner, M. Balogh, J. Vajo, Phase boundaries and reversibility of $LiBH_4/MgH_2$ hydrogen storage material, J. Phys. Chem. C. 111 (2007) 12881–12885.
[3] P. Mauron, F. Buchter, O. Friedrichs, A. Remhof, M. Bielmann, C. Zwicky, A. Zuttel, Stability and reversibility of $LiBH_4$, J. Phys. Chem. B 112 (2008) 906–910.
[4] E. Ronnebro, E. Majzoub, Calcium borohydride for hydrogen storage: catalysis and reversibility, J. Phys. Chem. B 111 (2007) 12045–12047.
[5] M. Chong, M. Mastuo, S. Orimo, T. Autrey, C. Jensen, Selective reversible hydrogenation of $Mg(B_3H_8)_2/MgH_2$ to $Mg(BH_4)_2$: pathway to reversible borane-based hydrogen storage? Inorg. Chem. 54 (2015) 4120–4125.
[6] P. Chen, Z. Xiong, J. Luo, J. Lin, K. Tan, Interaction of hydrogen with metal nitrides and imides, Nature 420 (2002) 302–304.
[7] Z. Huang, M. Eagles, S. Porter, E.G. Sorte, B. Billet, R.L. Corey, M.S. Conradi, J.-C. Zhao, Thermolysis and solid state NMR studies of NaB_3H_8, $NH_3B_3H_7$, and $NH_4B_3H_8$, Dalton Trans. 42 (2012) 701.
[8] Z. Huang, H.K. Lingam, X. Chen, S.H. Porter, A. Duo, P.M. Woodard, S.G. Shore, J.-C. Zhao, Synthesis, structural analysis, and thermal decomposition studies of $[(NH_3)_2BH_2]B_3H_8$, RSC Adv. 3 (2013) 7460–7465.
[9] Z. Huang, X. Chen, T. Yisgedu, J.-C. Zhao, S.G. Shore, High-capacity hydrogen release through hydrolysis of NaB_3H_8, Int. J. Hydrog. Energy 36 (2011) 7038–7042.
[10] G. Soloveichik, M. Andrus, Y. Gao, S. Kniajanski, J. Zhao, Magnesium borohydride as a hydrogen storage material: synthesis of unsolvated $Mg(BH_4)_2$, Int. J. Hydrog. Energy 34 (2009) 2144–2152.
[11] G. Severa, E. Ronnebro, C. Jensen, Direct hydrogenation of magnesium boride to magnesium borohydride: demonstration of >11 weight percent reversible hydrogen storage, Chem Comm. 46 (2010) 421–423.
[12] M. Chong, A. Karkamkar, T. Autrey, S. Orimo, S. Jalisatgi, C. Jensen, Reversible dehydrogenation of magnesium borohydride to magnesium triborane in the solid state under moderate conditions, Chem. Comm. 47 (2011) 1330–1332.
[13] L. Klebanoff, J. Keller, 5 Years of hydrogen storage research in the U.S. DOE metal hydride center of excellence (MHCoE), Int. J. Hydrog. Energy 38 (2013) 4533–4576.
[14] W. Luo, J. Wang, K. Stewart, M. Clift, K. Gross, Li–Mg–N–H: recent investigations and development, J. Alloy. Compd. 446-447 (2007) 336–341.
[15] H. Wu, Structure of ternary imide $Li_2Ca(NH)_2$ and hydrogen storage mechanisms in amide-hydride systems, J. Am. Chem. Soc. 130 (2008) 6515–6522.
[16] H. Wu, Strategies for the improvement of hydrogen storage properties of metal hydride materials, ChemPhysChem 9 (2008) 2157–2162.
[17] J. Wang, T. Liu, G. Wu, W. Li, Y. Liu, C. Araujo, P. Chen, Potassium-modified $Mg(NH_2)_2$/2LiH system for hydrogen storage, Angew. Chem. Int. Ed. 48 (2009) 5828–5832.
[18] G. Meisner, M. Scullin, M. Balogh, F. Pinkerton, M. Meyer, Hydrogen release from mixtures of lithium borohydride and lithium amide: a phase diagram study, J. Phys. Chem. B 110 (2006) 4186–4192.
[19] H. Wu, W. Zhou, T.J. Udovic, J.J. Rush, T. Yildirim, Structures and crystal chemistry of Li_2BNH_6 and $Li_4BN_3H_{10}$, Chem. Mater. 20 (2008) 1245–1247.
[20] H. Chu, Z. Xiong, G. Wu, J. Guo, T. He, P. Chen, Improved dehydrogenation properties of $Ca(BH_4)_2$-$LiNH_2$ combined system, Dalton Trans. 39 (2010) 10585–10587.
[21] M. Somer, S. Acar, C. Koz, I. Kokal, P. Hohn, R. Cardoso-GII, U. Aydemir, L. Akselrud, α- and β-$Na_2[BH_4][NH_2]$: two modifications of a complex hydride in the system $NaNH_2$–$NaBH_4$; syntheses, crystal structures, thermal analyses, mass and vibrational spectra, J. Alloy. Compd. 491 (2010) 98–105.
[22] T. Noritake, K. Miwa, M. Aoki, M. Matsumoto, S. Towata, H. Li, S. Orimo, Synthesis and crystal structure analysis of complex hydride $Mg(BH_4)(NH_2)$, Int. J. Hydrog. Energy 38 (2013) 6730–6735.
[23] H. Wu, W. Zhou, K. Wang, T.J. Udovic, J.J. Rush, T. Yildirim, L. Bendersky, A. F. Gross, S.L.V. Atta, J.J. Vajo, F.E. Pinkerton, M.S. Meyer, Size effects on the hydrogen storage properties of nanoscaffolded $Li_3BN_2H_8$, Nanotechnology 20 (2009) 204002.
[24] G. Soloveichik, J. Her, P. Stephens, Y. Gao, J. Rijssenbeek, M. Andrus, J. Zhao, Ammine magnesium borohydride complex as a new material for hydrogen storage: structure and properties of $Mg(BH_4)_2 \cdot 2NH_3$, Inorg. Chem. 47 (2008) 4290–4298.
[25] J. Lars, M. Ley, Y. Lee, Y. Cho, M. Dornheim, J. Jensen, Y. Filinchuk, J. Jorgensen, F. Besenbacher, T. Jensen, Boron–nitrogen based hydrides and reactive composites for hydrogen storage, Mater. Today 17 (2014) 129–135.
[26] Z. Tang, Y. Tan, H. Wu, Q. Gu, W. Zhou, C. Jensen, X. Yu, Metal cation-promoted hydrogen generation in activated aluminium borohydride ammoniates, Acta Mater. 61 (2013) 4787–4796.
[27] M. Gobel, T. Klapotke, First structural characterization of guanidine, $HN=C(NH_2)_2$, Chem Comm. (2007) 3180–3182.
[28] A. Doroodian, J. Dengler, A. Genest, N. Rosch, B. Rieger, Methylguanidinium borohydride: an ionic-liquid-based hydrogen-storage material, Angew. Chem. Int. Ed. 49 (2010) 1871–1873.
[29] A.C. Larson, R.B. Von Dreele, General Structure Analysis System, Report LAUR 86-748, Los Alamos National Laboratory, NM, 1994.
[30] W. Zhou, H. Wu, M.R. Hartman, T. Yildirim, Hydrogen and methane adsorption in metal-organic frameworks: a high-pressure volumetric study, J. Phys. Chem. C 111 (2007) 16131–16137.
[31] P. Giannozzi, S. Baroni, N. Bonini, M. Calandra, R. Car, C. Cavazzoni, D. Ceresoli, G.L. Chiarotti, M. Cococcioni, I. Dabo, A. Dal Corso, S. Fabris, G. Fratesi, S. de Gironcoli, R. Gebauer, U. Gerstmann, C. Gougoussis, A. Kokalj, M. Lazzeri, L. Martin-Samos, N. Marzari, F. Mauri, R. Mazzarello, S. Paolini, A. Pasquarello, L. Paulatto, C. Sbraccia, S. Scandolo, G. Sclauzero, A.P. Seitsonen, A. Smogunov, P. Umari, R.M. Wentzcovitch, Quantum espresso: a modular and open-source software project for quantum simulations of materials, J. Phys.: Condens. Matter 21 (39) (2009) 395502.
[32] R. Car, M. Parrinello, Unified approach for molecular dynamics and density-functional theory, Phys. Rev. Lett. 55 (22) (1985) 2471–2474.
[33] G. Kresse, J. Furthmuller, J. Hafner, Ab Initio force constant approach to phonon dispersion relations of diamond and graphite, EPL (Europhys. Lett.) 32 (9) (1995) 729.
[34] I. Hwang, T. Drews, K. Seppelt, Mg $(NH_3)_6Hg_{22}$, a mercury intercalation compound, J. Am. Chem. Soc. 122 (2000) 8486–8489.
[35] Y. Yang, Y. Liu, H. Wu, W. Zhou, M. Gao, H. Pan, An ammonia-stabilized mixed-cation borohydride: synthesis, structure and thermal decomposition behavior, Phys. Chem. Chem. Phys. 16 (2014) 135–143.
[36] X. Kang, H. Wu, J. Luo, W. Zhou, P. Wang, A simple and efficient approach to synthesize amidoborane ammoniates: case study for $Mg(NH_2BH_3)_2(NH_3)_3$ with unusual coordination structure, J. Mater. Chem. 22 (2012) 13174–13179.
[37] H. Chu, G. Wu, Z. Xiong, J. Guo, T. He, P. Chen, Structure and hydrogen storage properties of calcium borohydride diammoniate, Chem. Mater. 22 (2010) 6021–6028.
[38] Y.S. Chua, H. Wu, W. Zhou, T.J. Uodovic, G. Wu, Z. Xiong, M.W. Wong, P. Chen, Monoammoniate of calcium amidoborane: synthesis, structure, and hydrogen-storage properties, Inorg. Chem. 51 (2012) 1599–1603.
[39] S. Johnson, W. David, D. Royse, M. Sommariva, C. Tang, F. Fabbiani, M. Jones, P. Edwards, The monoammoniate of lithium borohydride, $Li(NH_3)BH_4$: an effective ammonia storage compound, Chem. Asian J. 4 (2009) 849–854.
[40] X. Zheng, G. Wu, W. Li, Z. Xiong, T. He, J. Guo, H. Chen, P. Chen, Releasing 17.8 wt% H_2 from lithium borohydride ammoniate, Energy Environ. Sci. 4 (2011) 3593–3600.
[41] A. Paolone, F. Teocoli, S. Sanna, O. Palumbo, T. Autrey, Temperature dependence of the infrared spectrum of ammonia borane: librations, rotations, and molecular vibrations, J. Phys. Chem. C 117 (2013) 729–734.
[42] Y. Yan, A. Remhof, D. Rentsch, A. Zuttel, Chem. Commun. 51 (2015) 700–702.
[43] T. Ichikawa, N. Hanada, S. Isobe, J. Phys. Chem. B 108 (2004) 7887.
[44] Y.H. Hu, E. Ruckenstein, J. Phys. Chem. A 107 (2003) 9737.
[45] Y. Guo, H. Wu, W. Zhou, X. Yu, Dehydrogenation tuning of ammine borohydrides using double-metal cations, J. Am. Chem. Soc. 13 (2011) 4690–4693.
[46] T. He, H. Wu, J. Chen, W. Zhou, G. Wu, Z. Xiong, J. Chen, T. Zhang, P. Chen, Alkali and alkaline-Earth metal borohydride hydrazinates: synthesis, structures and dehydrogenation, Phys. Chem. Chem. Phys. 15 (2013) 10487–10493.
[47] T. He, H. Wu, G. Wu, J. Wang, W. Zhou, Z. Xiong, J. Chen, T. Zhang, P. Chen, Borohydride hydrazinates: high hydrogen content materials for hydrogen storage, Energy Environ. Sci. 5 (2012) 5686–5689.
[48] S. Orimo, Y. Nakamori, G. Kitahara, Destabilization and enhanced dehydriding reaction of $LiNH_2$: an electronic structure viewpoint, Appl. Phys. A 79 (2004) 1765–1767.